Multicomponent Diffusion of Hydrogen-Bonding Solutes in a Polymer

Yossef A. Elabd
Dept. of Chemical Engineering, Johns Hopkins University, Baltimore, MD 21218

Timothy A. Barbari
Dept. of Chemical Engineering, University of Maryland, College Park, MD 20742

The diffusion of methyl ethyl ketone (MEK)/1-butanol (BOH) mixtures in polyisobutylene (PIB) was studied using time-resolved FTIR-ATR spectroscopy at varying mixture compositions. Diffusion coefficients and hydrogen-bonding interactions were quantitatively measured using this technique. In the MEK/BOH/PIB system, three species were identified from the infrared spectra, free MEK, an MEK-BOH complex, and a self-associated BOH cluster. The diffusion coefficient for the MEK-BOH complex was less than that for free MEK, but larger than the values determined for the BOH cluster. These results were compared to a numerical solution of a multicomponent transport model that explicitly accounts for solute − solute interactions to determine individual diffusion coefficients for all the species identified. In addition, the MEK/BOH/PIB results were compared to those for an MEK/acetonitrile (ACN) mixture, a nonhydrogen-bonding system, in PIB, to elucidate the differences between interacting and noninteracting systems.

Introduction

Understanding multicomponent diffusion in polymers at a molecular level is important for many applications, including membrane-based separations, selective-barrier materials, and fuel-cell technology. For a simple or binary system (solute(1)/polymer), there is a single diffusion coefficient that characterizes the transport process using a simple transient continuity equation:

$$\frac{\partial C_1}{\partial t} = D_1 \frac{\partial^2 C_1}{\partial z^2}, \tag{1}$$

where D_1 is defined as the diffusion coefficient of the solute in the polymer. Multicomponent systems, however, have traditionally been described under two similar mathematical frameworks: the generalized Stefan–Maxwell and Onsager formalisms (Maxwell, 1867; Stefan, 1872; Onsager, 1931; Cussler, 1976). In the Onsager framework, transport can be described by an array of diffusion coefficients through a multicomponent, transient form of the continuity equation:

$$\frac{\partial C_i}{\partial t} = \sum_{j=1}^{n-1} D_{ij} \frac{\partial^2 C_j}{\partial z^2}. \tag{2}$$

In this array of diffusion coefficients, the diagonal terms, D_{ii}, are referred to as "main-term" diffusion coefficients, and the off-diagonal terms, D_{ij} (where $i \neq j$), are called "cross-term" diffusion coefficients. The main-term diffusion coefficients are similar in magnitude to their respective binary diffusion coefficients and are sometimes referred to as pseudobinary values. The cross-term diffusion coefficients are somewhat vague in their interpretation, but in general, each one is a relative measure of the effect of one component's concentration gradient on the flux of another component or the system's deviation from the binary case (Cussler, 1976). For example, for a ternary system (solute(1)/solute(2)/polymer), the continuity equations would be:

$$\frac{\partial C_1}{\partial t} = D_{11} \frac{\partial^2 C_1}{\partial z^2} + D_{12} \frac{\partial^2 C_2}{\partial z^2} \tag{3}$$

Correspondence concerning this article should be addressed to T. A. Barbari.

$$\frac{\partial C_2}{\partial t} = D_{21}\frac{\partial^2 C_1}{\partial z^2} + D_{22}\frac{\partial^2 C_2}{\partial z^2}. \quad (4)$$

The Stefan–Maxwell framework results in a similar array of diffusion coefficients to describe the system. Both the generalized Onsager and Stefan–Maxwell formalisms can be derived from irreversible thermodynamics (Cussler, 1976).

In this study, the diffusion of two solutes capable of hydrogen bonding was investigated. In the Onsager framework just presented, there is no way to account for the complexation and self-association that can result from hydrogen bonding. Therefore, little to no insight into the nature and extent of these interactions can be inferred from the magnitudes of the main-term and cross-term coefficients if applied to this problem. If chemical potential gradients are used in the Onsager formalism, these interactions can be captured through thermodynamic expressions relating chemical potential to concentration. However, questions still remain as to the physical meaning of the diffusion coefficients. Therefore, an alternative approach was sought to account for hydrogen bonding explicitly in order to obtain transport parameters with simple yet physical interpretations.

Experimentally, FTIR-ATR spectroscopy, NMR imaging, diffusion cells, and capillary column inverse gas chromatography have been used to measure multicomponent diffusion in a polymer (Grinsted and Koenig, 1992; Balik and Simendinger, 1988; Hong et al., 1998; Danner et al., 1998; Zielinski and Hanley, 1999). However, the ability to quantitatively measure interactions among diffusing components has not yet been demonstrated. The ability to measure multicomponent diffusion and determine how solute–solute interactions affect the overall transport rates could aid in the optimization of transport-related polymer processes.

The focus of this study was not only to quantify multicomponent diffusion in a polymer, but also to measure quantitatively the interactions among the species during the transport process. Through shifts in the infrared spectrum, FTIR-ATR spectroscopy has the ability to measure the extent of chemical interactions, such as hydrogen bonding, among the different species during the transport process. Recently, Elabd and Barbari (2001) quantified both the diffusion coefficient of a solute in a polymer and its interaction to the polymer using time-resolved FTIR-ATR spectroscopy. In this study, the diffusion of and interaction between multiple solutes in a polymer, a hydrogen-bonding mixture of methyl ethyl ketone (MEK) and *1*-butanol (BOH) in polyisobutylene (PIB), were investigated with FTIR-ATR spectroscopy. In addition, the experimental results were compared to a multicomponent model that explicitly accounts for the specific solute–solute interactions.

Model Development

Since O—H bonds in BOH can either self-associate or interact with the C=O bonds in MEK through hydrogen bonding, this system presents a very complex scenario for diffusion at the molecular level. MEK and BOH molecules interact reversibly to form an MEK-BOH complex. One approach to modeling this system is to incorporate these interactions and describe the diffusion of species that are created through hydrogen bonding and identifiable from FTIR-ATR spectroscopy. As will be shown experimentally below, there is no quantifiable infrared band for single BOH molecules, only for self-associated BOH clusters. The diffusion of MEK and BOH then can be treated in terms of the diffusion of three species, free or monomeric MEK, clustered BOH, and an MEK-BOH complex, as illustrated in Figure 1.

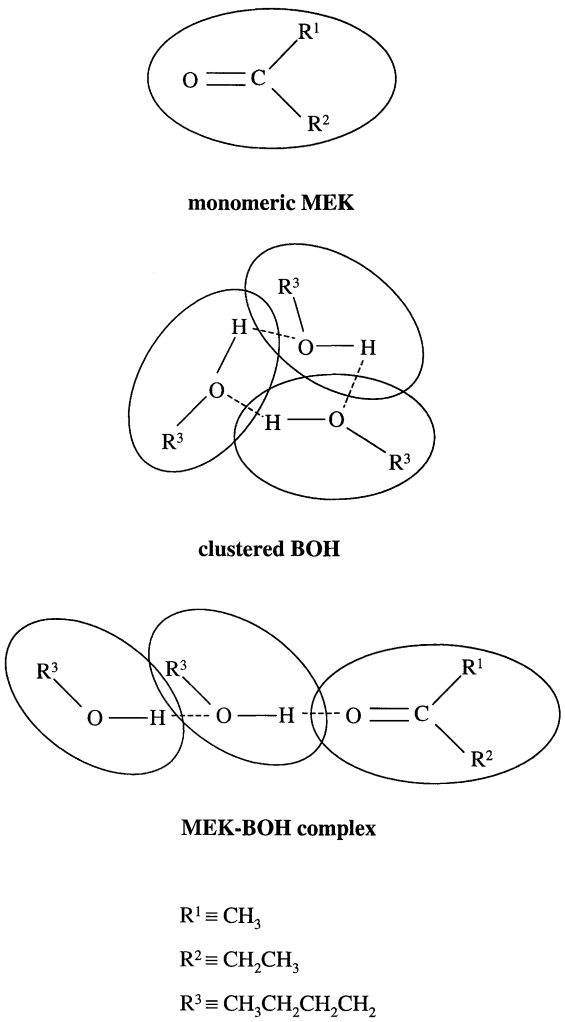

Figure 1. Multiple components, free or monomeric MEK, clustered BOH, and an MEK-BOH complex, involved in the diffusion of interacting mixture of MEK/BOH in PIB.

All three components have the capability of diffusing across the membrane.

To describe this process mathematically, a diffusion model with an equilibrium reaction between free MEK, clustered BOH, and the MEK-BOH complex was developed. The reaction can be written as

$$A + (n/m)B_m \underset{k_r}{\overset{k_f}{\rightleftharpoons}} AB_n, \quad (5)$$

where A, B_m, and AB_n represent the MEK monomer, BOH cluster, and MEK-BOH complex, respectively. In addition, m

and n refer to the size of the BOH cluster (number of BOH monomers) and MEK-BOH complex (number of BOH monomers per MEK), respectively. The one-dimensional continuity equations for these species are

$$\frac{\partial C_A}{\partial t} = D_{A,eff}\frac{\partial^2 C_A}{\partial z^2} = D_A\frac{\partial^2 C_A}{\partial z^2} + r_A \tag{6}$$

$$\frac{\partial C_{B_m}}{\partial t} = D_{B_m,eff}\frac{\partial^2 C_{B_m}}{\partial z^2} = D_{B_m}\frac{\partial^2 C_{B_m}}{\partial z^2} + (n/m)r_A \tag{7}$$

$$\frac{\partial C_{AB_n}}{\partial t} = D_{AB_n,eff}\frac{\partial^2 C_{AB_n}}{\partial z^2} = D_{AB_n}\frac{\partial^2 C_{AB_n}}{\partial z^2} - r_A, \tag{8}$$

where, if hydrogen bonding is treated as elementary,

$$r_A = -k_f C_A C_{B_m}^{n/m} + k_r C_{AB_n}, \tag{9}$$

and z and t correspond to the distance in the polymer and time, respectively. In Eqs. 6–9, C_A, C_{B_m}, and C_{AB_n}, are the concentrations of MEK monomer, BOH cluster, and MEK-BOH complex, respectively, while $D_{A,eff}$, $D_{B_m,eff}$, $D_{AB_n,eff}$, and D_A, D_{B_m}, and D_{AB_n} are their respective effective and individual diffusion coefficients. Additionally, k_f and k_r are forward and reverse rate constants, respectively, and the equilibrium constant is given as

$$K = \frac{k_f}{k_r}. \tag{10}$$

Since FTIR-ATR spectroscopy has the capability of measuring the concentrations of individual species, the effective or overall diffusion coefficient of each penetrant was determined. To determine the relationship between individual and effective diffusion coefficients, the experimental data were then compared to the numerical solution of Eqs. 6–9, and to data for the noninteracting system.

Effective diffusion coefficient determination

Under the assumptions of weak infrared absorption, negligible changes in the polymer refractive index (dilute concentrations) and the thick-film approximation (Elabd, 2000), the absorbance in FTIR-ATR spectroscopy can be related to the concentration at the polymer–ATR element interface (see Figure 2) through the expression

$$A(t) = \epsilon^* d_p C(t, z=0), \tag{11}$$

where $A(t)$ and $C(t,\ z\ =\ 0)$ are the integrated infrared absorbance and concentration, respectively; ϵ^* is the effective extinction coefficient for FTIR-ATR spectroscopy; and d_p is the depth of infrared radiation penetration into the polymer film. The effective diffusion coefficient can be determined from a regression of experimental ATR absorbance data to an analytical solution of Fick's second law, which can be expressed as (Elabd, 2000)

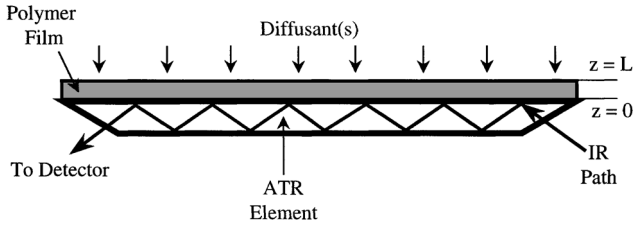

Figure 2. ATR element.

$$\frac{A_i(t)}{A_{i,\mathrm{eq}}} = \frac{C_i(t, z=0)}{C_{i,\mathrm{eq}}}$$

$$= 1 - \frac{4}{\pi}\sum_{n=0}^{\infty}\frac{(-1)^n}{2n+1}\exp\left(\frac{-D_{i,\mathrm{eff}}(2n+1)^2\pi^2 t}{4L^2}\right), \tag{12}$$

where, for species i, $D_{i,\mathrm{eff}}$ is the effective diffusion coefficient, $A_{i,\mathrm{eq}}$ and $C_{i,\mathrm{eq}}$ are the integrated absorbance and concentration, respectively, at equilibrium, and L is the film thickness.

Individual diffusion coefficient determination

To determine the individual diffusion coefficients, the coupled species continuity equations (Eqs. 6–8) must be solved numerically. The following variables were used to convert the equations into dimensionless form, where $C_{T,\mathrm{eq}}$ is the total concentration of solute at equilibrium:

$$\left(C_{T,\mathrm{eq}} = C_{A,\mathrm{eq}} + mC_{B_m,\mathrm{eq}} + (n+1)C_{AB_n,\mathrm{eq}}\right)$$

$$\theta_A = \frac{C_A}{C_{T,\mathrm{eq}}} \tag{13}$$

$$\theta_{B_m} = \frac{C_{B_m}}{C_{T,\mathrm{eq}}} \tag{14}$$

$$\theta_{AB_n} = \frac{C_{AB_n}}{C_{T,\mathrm{eq}}} \tag{15}$$

$$\tau = \frac{D_A t}{L^2} \tag{16}$$

$$\zeta = \frac{z}{L}. \tag{17}$$

Recasting Eqs. 6–9 with the use of these dimensionless variables results in

$$\frac{\partial\theta_A}{\partial\tau} = \frac{\partial^2\theta_A}{\partial\zeta^2} - s_1\left(s_2\theta_A\theta_{B_m}^{n/m} - \theta_{AB_n}\right) \tag{18}$$

$$\frac{\partial\theta_{B_m}}{\partial\tau} = s_3\frac{\partial^2\theta_{B_m}}{\partial\zeta^2} - (n/m)s_1\left(s_2\theta_A\theta_{B_m}^{n/m} - \theta_{AB_n}\right) \tag{19}$$

$$\frac{\partial \theta_{AB_n}}{\partial \tau} = s_4 \frac{\partial^2 \theta_{AB_n}}{\partial \zeta^2} + s_1\left(s_2 \theta_A \theta_{B_m}^{n/m} - \theta_{AB_n}\right), \tag{20}$$

where

$$s_1 = \frac{k_r L^2}{D_A} \tag{21}$$

$$s_2 = K C_{T,\mathrm{eq}}^{n/m} \tag{22}$$

$$s_3 = \frac{D_{B_m}}{D_A} \tag{23}$$

$$s_4 = \frac{D_{AB_n}}{D_A}. \tag{24}$$

The initial conditions recast into dimensionless form (at $\tau = 0$ for all ζ) become:

$$\theta_A = 0 \tag{25}$$

$$\theta_{B_m} = 0 \tag{26}$$

$$\theta_{AB_n} = 0. \tag{27}$$

The boundary conditions at $\zeta = 0$ for all τ are

$$\frac{\partial \theta_A}{\partial z} = 0 \tag{28}$$

$$\frac{\partial \theta_{B_m}}{\partial z} = 0 \tag{29}$$

$$\frac{\partial \theta_{AB_n}}{\partial z} = 0, \tag{30}$$

and those at $\zeta = 1$ for all τ are

$$\theta_A = \theta_{A,\mathrm{eq}} \tag{31}$$

$$\theta_{B_m} = \theta_{B_m,\mathrm{eq}} \tag{32}$$

$$\theta_{AB_n} = \theta_{AB_n,\mathrm{eq}}. \tag{33}$$

In this model development, $\theta_{A,\mathrm{eq}}$, $\theta_{B_m,\mathrm{eq}}$, and $\theta_{AB_n,\mathrm{eq}}$ are not independent parameters, but are related through the equilibrium expression and the material balance:

$$s_2 = K C_{T,\mathrm{eq}}^{n/m} = \frac{\theta_{AB_n,\mathrm{eq}}}{\theta_{A,\mathrm{eq}} \theta_{B_m,\mathrm{eq}}^{n/m}} \tag{34}$$

$$\theta_{A,\mathrm{eq}} + m\theta_{B_m,\mathrm{eq}} + (n+1)\theta_{AB_n,\mathrm{eq}} = 1. \tag{35}$$

Therefore, only two of the four parameters, s_2, $\theta_{A,\mathrm{eq}}$, $\theta_{B_m,\mathrm{eq}}$, $\theta_{AB_n,\mathrm{eq}}$, can be specified independently. An implicit Crank–Nicolson finite difference algorithm was used to solve this system of equations, where the space domain was divided into 1,000 node points and a dimensionless time step of 0.0003 was used.

Experimental

Materials and sample preparation

Polyisobutylene (PIB) was purchased from Scientific Polymer Products, Inc. ($M_v = 4{,}700{,}000$ [GPC]; density = 0.92 g/cm^3; refractive index = 1.51; $T_g = -64$°C). The remaining chemicals used in this study, methyl ethyl ketone (MEK), *1*-butanol (BOH), acetonitrile (ACN), and toluene, were purchased from Aldrich Chemical Company, Inc., with 99.5% purity and used as received. The physical properties of the solutes, MEK, BOH, and ACN, are listed in Table 1.

To obtain polymer film samples for the FTIR-ATR experiments, a 3 wt % solution of PIB in toluene was cast onto a level ATR crystal and dried for 48 h in a fume hood. After drying, the films were placed in a vacuum oven for 48 h at 150°C to remove residual solvent. Separate samples, with film thicknesses (measured with a micrometer) in the range of 30 to $50 \pm 2.5\,\mu$m, were prepared for each spectroscopic experiment. No residual toluene was detected spectroscopically in the film attached to the ATR crystal.

Diffusion experiments

Infrared spectra for the diffusion experiments were obtained with a Mattson Research Series 1 FTIR spectrometer with a horizontal, temperature-controlled ATR cell purchased from Graseby Specac, Inc. The multiple-reflection ATR element (shown in Figure 2) (Graseby Specac, Inc.) was a zinc selenide trapezoid ($70 \times 10 \times 6$ mm) with entry and exit faces beveled at a 45° angle of incidence for the IR beam and with a refractive index of 2.4. Infrared radiation absorbs at the ATR element–polymer interface, and is detected with a liquid nitrogen-cooled, mercury–cadmium–telluride (MCT) detector. All spectra were collected with 32 scans, a 4-cm^{-1} resolution, and a 46-s sampling time, and they were corrected by background subtraction of the ATR element spectrum.

All diffusion and sorption experiments were conducted at 23 ± 1°C with different liquid mixture compositions expressed in ratios of mole fractions: 0:1, 0.2:0.8, 0.3:0.7, 0.4:0.6, 0.5:0.5, 0.6:0.4, 0.7:0.3, 0.8:0.2, and 1:0 MEK:BOH and 0:1, 0.3:0.7, 0.5:0.5, 0.7:0.3, and 1:0 MEK:ACN, where mole fraction is defined as the moles of one component to the total moles of the mixture. Liquid sorption (mass uptake) experiments were conducted at each mixture composition to determine the total concentration at equilibrium by saturating polymer samples (three samples at every mixture composition) weighing approximately 0.5–1 g in each liquid mixture. After one week, samples were removed, excess liquid was blotted from the surface of each sample, and the difference in mass (solute mass uptake) was determined using a Mettler balance with ± 0.0001-g precision.

Table 1. Molecular Weights, Boiling Temperatures, Densities, and Molar Volumes of Solutes

Penetrant	MW (g/mol)	T_b (°C)	ρ (g/cm^3)	$\bar{V}$ (cm^3/mol)
MEK	72.11	80	0.805	89.6
BOH	74.12	117.7	0.810	91.5
ACN	41.05	81–82	0.786	52.2

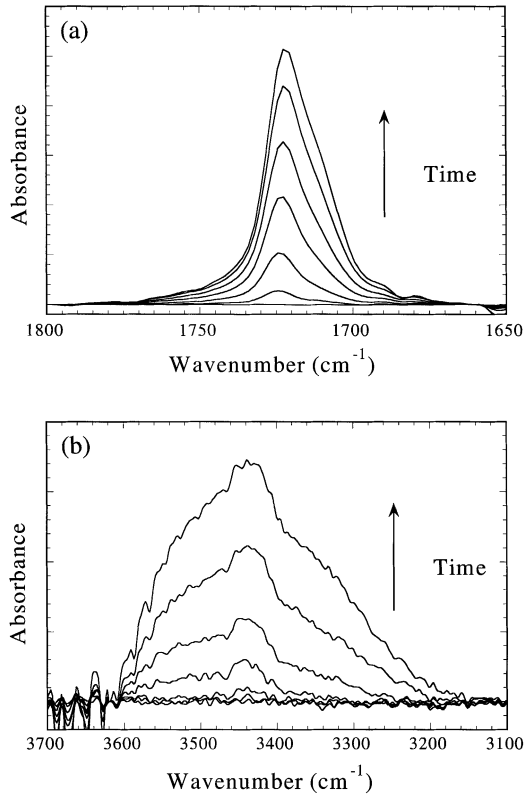

Figure 3. Time-resolved (a) C=O and (b) O—H absorbance spectra for 0.5:0.5 MEK:BOH in PIB at 23°C.

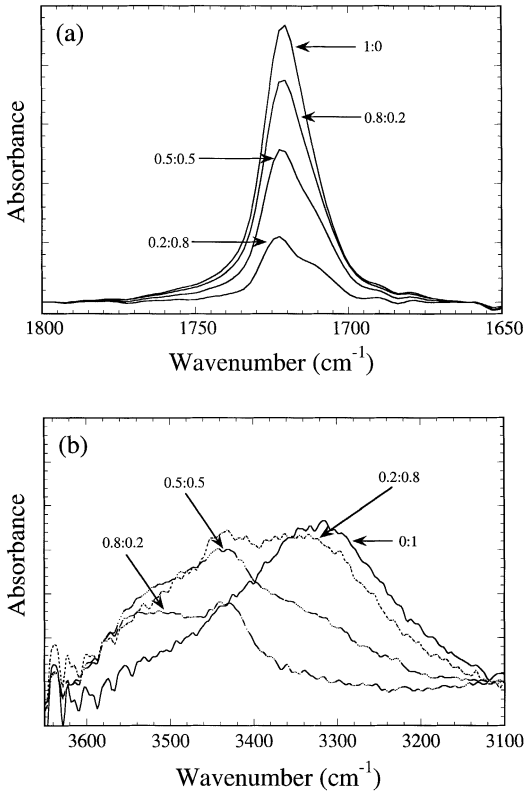

Figure 4. Equilibrium (a) C=O absorbance spectra and (b) O—H absorbance spectra of MEK/BOH in PIB at 23°C.

Numbers on graph correspond to concentration of the liquid mixture, MEK:BOH mole fraction ratio.

Results and Discussion

Structural analysis

Both the carbonyl (C=O) and hydroxyl (O—H) vibrational bands, in particular the stretching frequencies, of the infrared spectra were used for the MEK/BOH mixtures in PIB, in order to identify the diffusing species in this system. Both the C=O stretch and the O—H stretch are sensitive to hydrogen bonding. The O—H bond in particular shifts significantly in wavenumber with different hydrogen-bonding states or strengths. Figure 3 shows several C=O and O—H spectra at different times for one diffusion experiment, 0.5:0.5 MEK:BOH in PIB. In Figure 3a, in addition to the main peak at 1722 cm^{-1}, there is a C=O shoulder at 1711 cm^{-1} that is indicative of hydrogen bonding and similar to one observed in an earlier study (Elabd and Barbari, 2001). This figure indicates that both free MEK and an MEK-BOH complex are present in PIB. Figure 3b shows several peaks, each of which represents a different hydrogen bonding state. To clarify the complexities in the infrared spectra, for Figure 3b in particular, the equilibrium spectra for the C=O and O—H stretches at different liquid mixture compositions, 1:0, 0.8:0.2, 0.5:0.5, 0.2:0.8, and 0:1 MEK:BOH in PIB, are compared in Figure 4. For pure MEK in Figure 4a, a single C=O peak at 1722 cm^{-1} is evident, which is consistent with a study conducted by Hong et al. (1997). Only MEK monomer is present in PIB with no interactions with itself or the polymer. As BOH is added, there is the expected decrease in intensity with decreasing MEK concentration in the mixture, but the shoulder representing the hydrogen-bound MEK-BOH complex becomes more distinguishable at higher BOH concentrations. In Figure 4b, for pure BOH, a broad OH peak at 3330 cm^{-1}, representing self-associated BOH clusters, dominates the spectrum. If present in measurable quantities, free BOH molecules in PIB would be represented by a band at 3620 cm^{-1} (Bellamy, 1958; Avram and Mateescu, 1972; Lin-Vien et al., 1991), which was not evident in this study. Given the nonpolar environment of PIB, the amount of the highly polar, free BOH is expected, from thermodynamic arguments, to be very small compared to hydrogen-bonded BOH and was taken to be negligible here. As the concentration of MEK increases in the mixture, other peaks appear at higher wavenumbers, and at 0.8:0.2 MEK:BOH, the peak at 3330 cm^{-1} is no longer present.

In order to determine the structures associated with the peaks in Figure 4, the equilibrium C=O and O—H spectra were deconvoluted using a curve-fitting program provided in the Advanced FIRST (Mattson Instruments, Inc.) software package. The resulting synthetic peaks for the experiment with a liquid mixture composition of 0.5:0.5 MEK:BOH in PIB is shown in Figure 5. Figure 5a illustrates the expected peaks at 1722 cm^{-1} and 1711 cm^{-1} (Lorentzian contours), representing the MEK monomer and the MEK hydrogen-bound complex, respectively (Elabd and Barbari, 2001). The

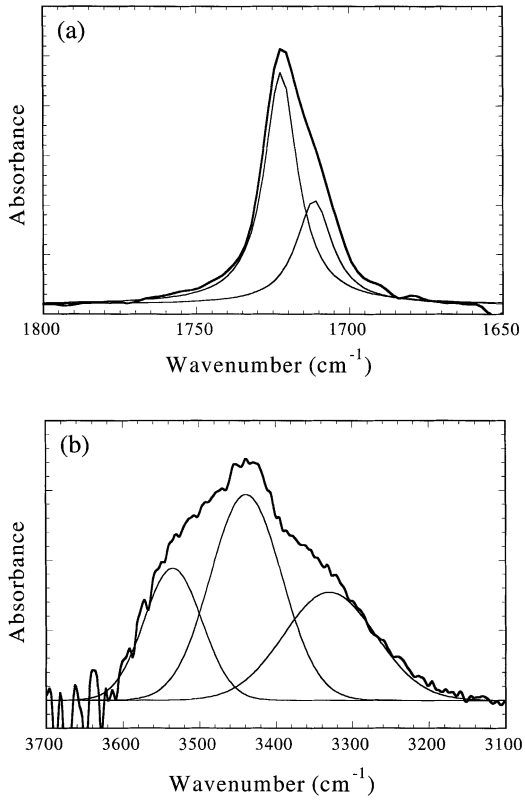

Figure 5. Deconvolution of equilibrium (a) C=O and (b) O—H absorbance spectrum for 0.5:0.5 MEK:BOH in PIB at 23°C.

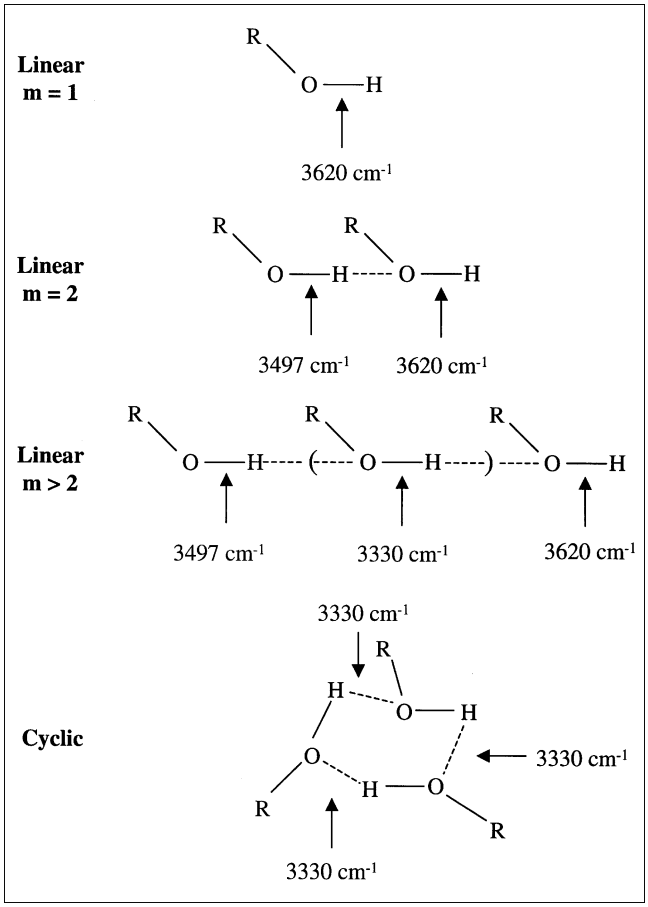

Figure 6. Designated peak locations for different hydrogen-bonding states of alcohol clusters.

deconvolution of the O—H spectrum (Gaussian contours), in Figure 5b, reveals three peaks, located at 3330, 3439, and 3535 cm^{-1}. The deconvolution of the C=O and O—H spectra using Lorentzian and Gaussian contours, respectively, was confirmed by fitting the spectra with the Lorentzian/Gaussian percentage allowed to be a fitting parameter, which resulted in a percentage always greater than 99% Lorentzian for the C=O spectra, and always greater than 99% Gaussian for the O—H spectra. Each of the peak locations in the O—H spectrum can be attributed to different hydrogen-bonding states of the O—H bond in BOH. It is well known that peak shifts in infrared spectra can be directly related to hydrogen-bond length or strength.

Figure 6 depicts bond assignments for various alcohol cluster sizes and structures (Bellamy, 1958; Avram and Mateescu, 1972; Lin-Vien et al., 1991). The monomer O—H stretch is located at 3620 cm^{-1}, which is also the location of the terminal O—H in self-associated linear chains. The greater the shift from this location to lower wavenumbers, the stronger the hydrogen bond. Hence, the O—H group that is involved in hydrogen bonding on both sides experiences the greatest shift in the infrared. When BOH self-associates as a cyclic cluster, all O—H groups are hydrogen bound on both sides and only one peak location appears, at 3330 cm^{-1}. This form of self-association is consistent with the experimental results for pure BOH in PIB (Figure 4b), and suggests that BOH diffuses as a cyclic self-associated cluster. The other peak locations, 3439 and 3535 cm^{-1}, that are seen in the MEK-BOH mixtures, can be attributed to different hydrogen-bonding states of the MEK-BOH complex. Figure 7 depicts peak locations for various complex sizes. As was the case for associated alcohols, the O—H peak with the greater shift in the complex, 3439 cm^{-1}, is the stronger or shorter hydrogen bond, and is evident for $n \geq 2$.

Diffusion analysis

If the assignment of peak locations in Figure 7 is correct, then the infrared peaks located at 1711, 3439, and 3535 cm^{-1} should all represent the same molecular species, a MEK-BOH complex, and the time rate of change for these three absorbances should be the same. To confirm this hypothesis, deconvolution of the peaks at equilibrium (shown in Figure 5) was conducted at each time point for every experiment. Figure 8a shows the results from the peak-fitting algorithm, time-resolved normalized integrated absorbances for five peaks, 1722, 1711, 3439, 3535 and 3330 cm^{-1}, for the 0.5:0.5 MEK:BOH experiment. The integrated areas of the peaks located at 1711, 3439 and 3535 cm^{-1} increase in time at the same rate, verifying the hypothesis that all three peaks represent the same molecular species, the MEK-BOH complex. Identical results were obtained at each mixture composition and in all of the experiments. In addition, Figure 8a shows

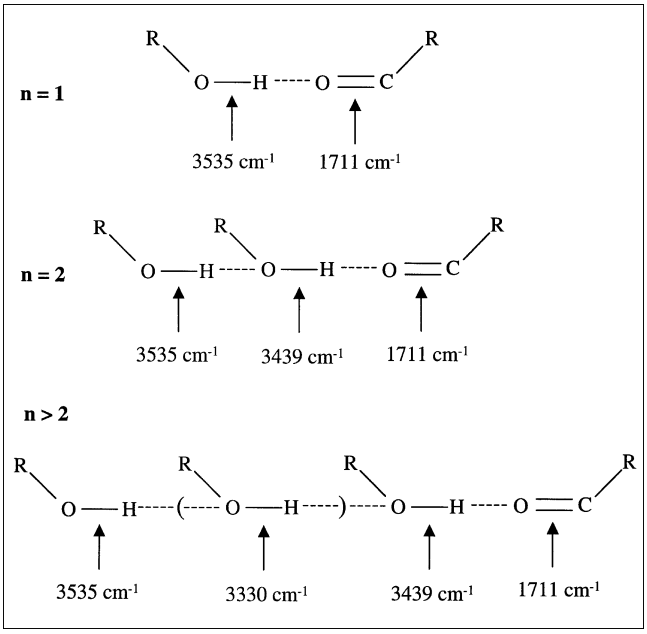

Figure 7. Designated peak locations for different hydrogen-bonding states alcohol–ketone complexes.

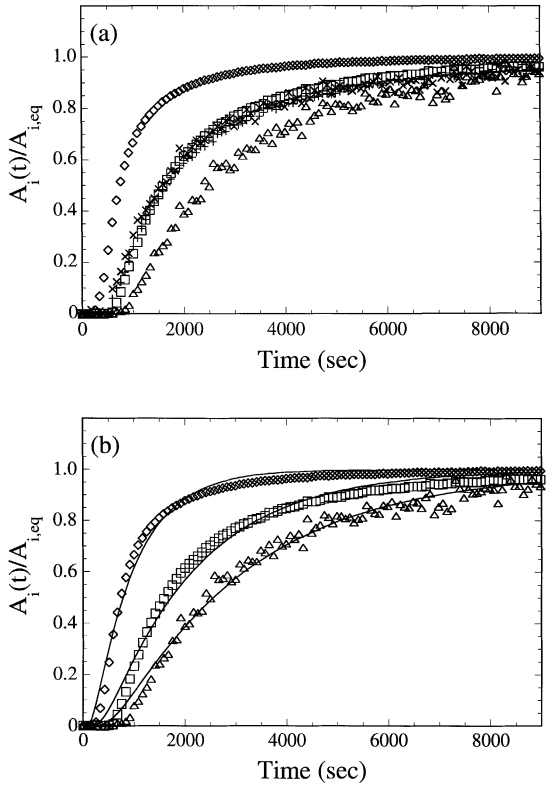

Figure 8. Time-resolved normalized integrated absorbance for separate components.

(a) MEK, 1722 cm^{-1} (◇), BOH cluster, 3330 cm^{-1} (△), and MEK-BOH complex, 1711 cm^{-1} (□), 3439 cm^{-1} (+), and 3535 cm^{-1} (×); (b) MEK, BOH cluster, and MEK-BOH complex regressed to the ATR solution, Eq. 12, (solid line) for the determination of effective diffusion coefficients.

that free MEK (1722 cm^{-1}) diffuses the fastest, followed by the MEK-BOH complex (1711, 3439 and 3535 cm^{-1}), and then the BOH cluster (3330 cm^{-1}).

The integrated absorbances were regressed to the transient ATR solution (Eq. 12) to determine the effective diffusion coefficient of each species. The diffusion of each species is Fickian, shown in Figure 8b for 0.5:0.5 MEK:BOH, for all experiments conducted at all mixture concentrations. The effective diffusion coefficients of all three species, MEK, MEK-BOH complex, and BOH cluster, are plotted against MEK mole fraction in the liquid mixture in Figure 9, where the error bars represent the standard deviation of three to six experiments conducted at each mixture composition. Each diffusion coefficient increases exponentially with MEK mole fraction, which is consistent with the basic ideas of free-volume theory (Cohen and Turnbull, 1959; Macedo and Litovitz, 1965; Chung, 1966), provided the total concentration of penetrant in the polymer increases linearly with increasing MEK mole fraction in the liquid mixture. To test this condition, the total concentration of penetrant in the polymer for every liquid mixture composition was measured from liquid-mass uptake experiments, shown in Figure 10. These results show that the total concentration of the mixture in the polymer increases linearly with increasing MEK mole fraction.

It is interesting to note that the effective diffusion coefficient for the BOH cluster in the absence of MEK from the extrapolation of the line in Figure 9 is approximately double that of the experimental value. It is feasible that the average size of the BOH cluster may increase at higher BOH concentrations. Several studies have shown that the diffusion coefficient of water and certain alcohols in polymers can decrease with increasing concentration (Aminabhavi and Khinnavar, 1993; Hsu et al., 1993). Investigators have interpreted this as an increase in cluster size with increasing concentration, which results in lower diffusion coefficients.

Application of numerical solution

In order to understand the effects of solute–solute interactions on multicomponent diffusion in polymers, a numerical solution was obtained to compare individual diffusion coefficients with effective values. The coupled equations, Eqs. 18–20, were solved under the condition of local equilibrium by setting the value of s_1 ($k_r L^2/D_A$) to 1,000 (Kasargod and Barbari, 1997). The open symbols in Figure 11 represent concentration profiles that were generated numerically for all three species using the following values: $n = 2$, $m = 4$, $D_A = 4.0 \times 10^{-9}$ cm^2/s, $s_3 = 0.25$, $s_4 = 0.33$, $\theta_{A,\mathrm{eq}} = 0.4$, and $\theta_{B_m,\mathrm{eq}} = 0.1$, while s_2 and $\theta_{AB_n,\mathrm{eq}}$ were determined from Eqs. 34 and 35. The value chosen for m is consistent with alcohol cluster sizes in low molecular-weight solvents (Prausnitz et al., 1986). The value of n was chosen to keep the complex size smaller than the cluster, since the experimental data indicate that the transport rate for the complex is faster than that for the cluster. Each normalized concentration profile generated was then regressed to the analytical solution of Fick's second law, Eq. 12, in order to determine the effective

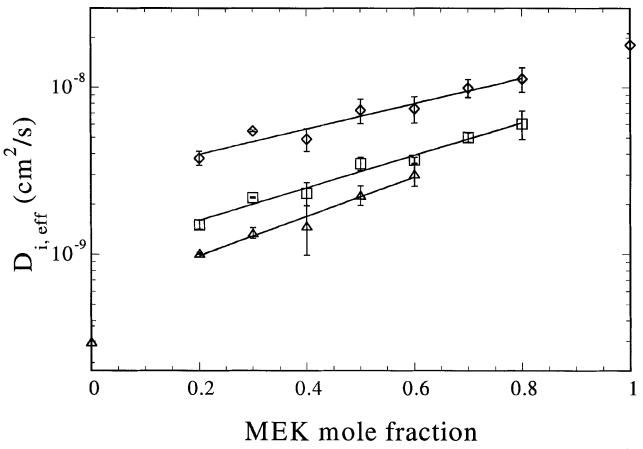

Figure 9. Effective diffusion coefficients for MEK (◇), MEK-BOH complex (□), and BOH cluster (△) vs. MEK mole fraction in the liquid mixture.

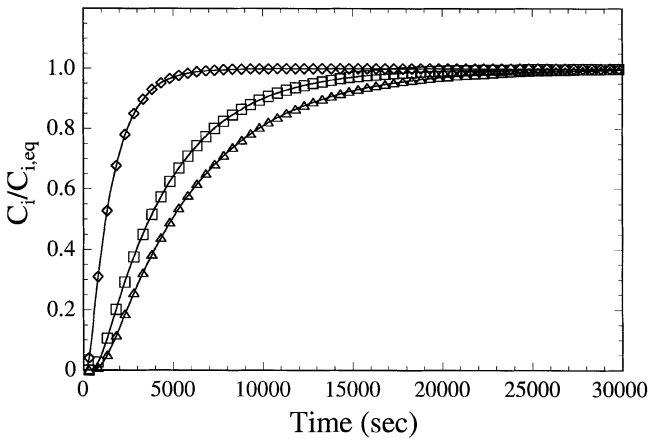

Figure 11. Comparison of individual and effective diffusion coefficients for all three species.

MEK (◇), MEK-BOH complex (□), and BOH cluster (△); open symbols and solid lines represent the individual and effective values, respectively.

diffusion coefficients. Deviations between individual diffusion coefficients (fixed through the numerical simulations) and effective diffusion coefficients (regressed to Fick's second law) would reveal the effects of interactions on diffusion. The fixed individual and regressed effective diffusion coefficients (see Figure 11) were the same, implying that Fick's second law can be used for each species under local equilibrium conditions. Similar results were obtained at other values of n, m, D_A, s_3, s_4, $\theta_{A,\mathrm{eq}}$ and $\theta_{B_m,\mathrm{eq}}$.

Comparison to a noninteracting system

To further elucidate the role of solute–solute interactions on multicomponent diffusion, mixtures of MEK/ACN in PIB, a noninteracting system, were studied and compared to MEK/BOH in PIB. Figure 12 shows the IR spectrum at equilibrium for one particular experiment, 0.3:0.7 MEK:ACN. The C=O peak (1722 cm^{-1}) is much greater than the C≡N peak (2253 cm^{-1}), because ACN has a low solubility in PIB and the nitrile stretching band absorbs weakly in the infrared. As a result, the C≡N spectra could not be quantified accurately. However, these experiments can be used to determine the diffusion coefficients of MEK in a multicomponent system with no solute–solute interactions at various liquid mixture concentrations for comparison with those for MEK in the MEK/BOH/PIB system. The total concentration for MEK/ACN liquid mixtures in PIB, determined from liquid-mass uptake experiments, is shown in Figure 13 at various liquid-phase MEK concentrations.

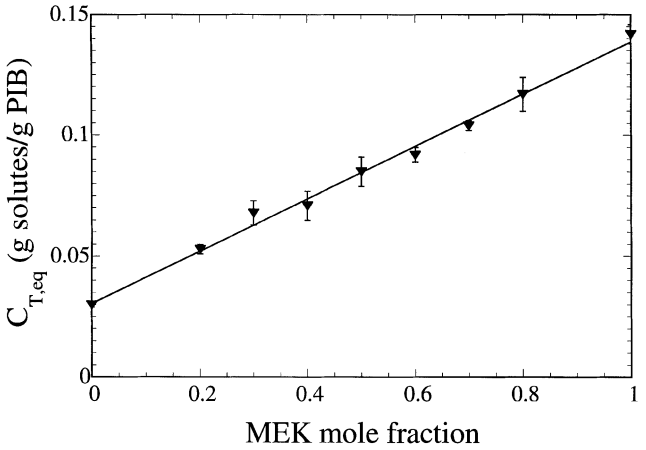

Figure 10. Total concentration of MEK/BOH penetrant mixture in PIB vs. MEK mole fraction in the liquid mixture.

From the basic concepts of free-volume theory (Cohen and Turnbull, 1959; Macedo and Litovitz, 1965; Chung, 1966), the diffusion coefficient at a fixed temperature is a function of the amount of free volume in a particular system, suggesting that the diffusion coefficient for MEK in PIB is independent of the nature of the components responsible for creating the additional free volume. If this is true, then the diffusion coefficient for MEK in the MEK/BOH/PIB system should be the same as that in the MEK/ACN/PIB system at the same system free volume, provided that all interactions have been accounted for correctly. All of the diffusants in this study have approximately the same mass density (see Table 1). Therefore, the total mass concentration of the mixture is a measure of the total volumetric swelling in the system, assuming no volume change upon mixing. Figure 13 suggests that the concentration of ACN is very small relative to that of MEK, since within experimental error, the total concentration is zero at a MEK mole fraction of zero (ACN mole fraction of one). As a result, ACN does not contribute measurably to the swelling in the system. Since the molar volumes of MEK and BOH are nearly identical, it is reasonable to assume that the occupied volume is also similar. Therefore, the volumetric swelling (reflected in total mass concentration) in both the MEK/ACN/PIB and MEK/BOH/PIB systems is a measure of additional free volume, and the MEK diffusion coeffi-

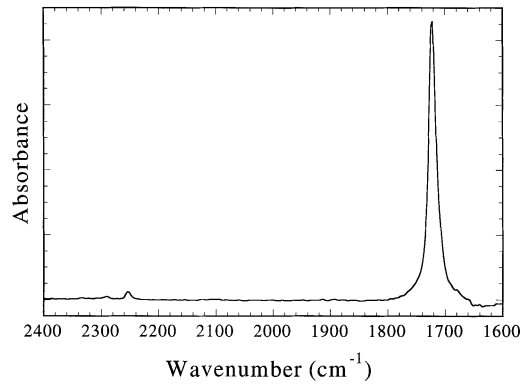

Figure 12. Equilibrium spectra for 0.3:0.7 MEK:ACN in PIB at 23°C.

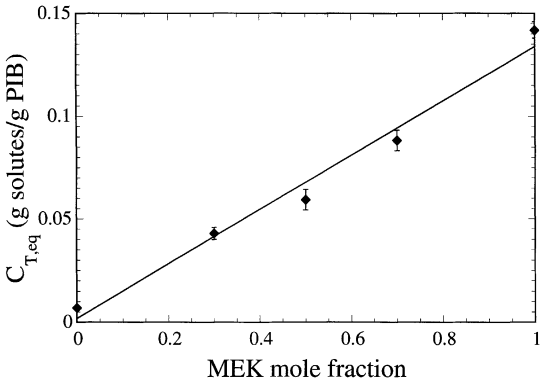

Figure 13. Total concentration of MEK/ACN penetrant mixture in PIB vs. MEK mole fraction in liquid mixture.

cients in each system should be equal at the same total mass concentration. The diffusion coefficients for MEK in both systems are plotted vs. the total concentration of the mixture in Figure 14. The results demonstrate that the MEK diffusion coefficient is only dependent on total system free volume, represented here by total mass concentration of the

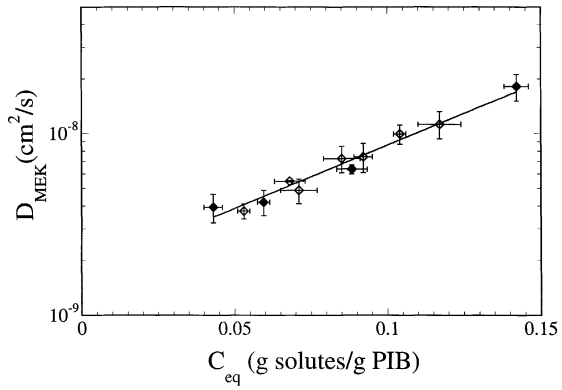

Figure 14. Diffusion coefficients for MEK in the MEK/BOH/PIB system (◇) and in the MEK/ACN/PIB system (♦) vs. total mixture concentration.

mixture, and that accounting for hydrogen-bonding interactions explicitly results in the correct individual diffusion coefficient for MEK.

If the diffusion coefficient for MEK had been measured with conventional techniques, the resulting value would have been a concentration-weighted average between the MEK and MEK-BOH diffusion coefficients determined in this study from FTIR-ATR spectroscopy. These weighted values would be lower than those in Figure 14, reinforcing the advantages of using FTIR-ATR spectroscopy to more fully elucidate transport mechanisms in complex systems.

Local equilibrium

To confirm the local equilibrium assumption in the modeling arguments, the absorbance values for all three species should be related at all times through the equilibrium constant, which can be written as

$$K = \frac{C_{AB_n}}{C_A C_{B_m}^{n/m}}. \tag{36}$$

Equation 36 relates the individual concentrations to the equilibrium constant (K) and the ratio of MEK-BOH complex size to BOH cluster size (n/m). Substitution of Eq. 11 into the local equilibrium expression, Eq. 36, leads to an equation that relates the experimental integrated absorbances at all times to both K and n/m

$$K = \frac{\left(\frac{A_{AB_n}}{\epsilon^*_{AB_n} d_{p_{AB_n}}}\right)}{\left(\frac{A_A}{\epsilon^*_A d_{p_A}}\right)\left(\frac{A_{B_m}}{\epsilon^*_{B_m} d_{p_{B_m}}}\right)^{n/m}}. \tag{37}$$

In Eq. 37, A_A, A_{AB_n}, and A_{B_m} are the integrated absorbances for MEK, MEK-BOH complex, and BOH cluster, respectively. Also, ϵ_i^* and d_{pi} are the effective extinction coefficient and depth of penetration, respectively, for each respective component. Equation 37 can be rearranged to

$$\frac{A_{AB_n}}{A_A} = K\left(\frac{\epsilon^*_{AB_n} d_{p_{AB_n}}}{\epsilon^*_A d_{p_A}}\right)\left(\frac{A_{B_m}}{\epsilon^*_{B_m} d_{p_{B_m}}}\right)^{n/m}, \tag{38}$$

and further to

$$\ln\left(\frac{A_{AB_n}}{A_A}\right) = \frac{n}{m}\ln\left(A_{B_m}\right) + \ln\left[K\left(\frac{\epsilon^*_{AB_n} d_{p_{AB_n}}}{\epsilon^*_A d_{p_A}}\right)\left(\frac{1}{\epsilon^*_{B_m} d_{p_{B_m}}}\right)^{n/m}\right], \tag{39}$$

where both K (from the intercept) and n/m (slope) can be determined from a log–log plot of A_{AB_n}/A_A vs. A_{B_m}, shown in Figure 15. In this figure, the data are well regressed linearly for all times during the diffusion experiment, confirm-

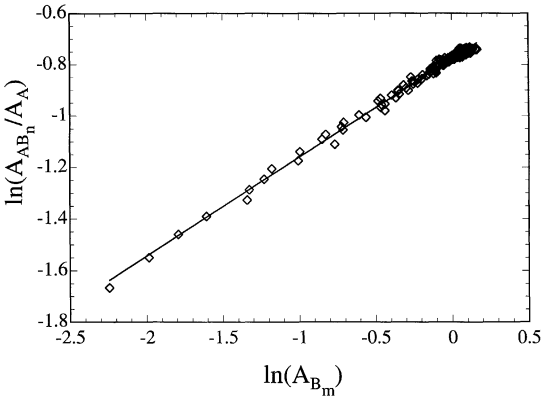

Figure 15. Log-log plot of A_{AB_n}/A_A vs. A_{B_m} for the confirmation of local equilibrium.

Table 2. Values of Intercept and Slope (n/m) from Local Equilibrium Calculation (Eq. 39)

MEK Mole Fraction	Intercept	Slope (n/m)
0.2	0.278 ± 0.004	0.418 ± 0.012
0.3	0.362 ± 0.048	0.396 ± 0.049
0.4	0.467 ± 0.137	0.365 ± 0.061
0.5	0.515 ± 0.125	0.337 ± 0.047
0.6	0.683 ± 0.153	0.400 ± 0.024

ing the local equilibrium assumption in Eq. 36. Values of the intercept and slope (n/m) were calculated for each mixture composition, and the results are shown in Table 2. The intercept increases with increasing MEK mole fraction, while the slope (n/m) remains relatively constant over this concentration range.

Conclusions

In this study, the diffusion of a hydrogen-bonding mixture in a polymer was examined both experimentally (FTIR-ATR spectroscopy) and numerically. The key result, as it pertains to the area of multicomponent diffusion in polymers, is that the diffusion can be both measured and modeled physically in terms of the species that result from these interactions (MEK-BOH complex and BOH cluster). Additionally, the ability to measure each component at all times can be used to confirm the local equilibrium assumption often assumed in diffusion analysis. Comparing the experimental results to the numerical solution clearly demonstrated that effective and individual diffusion coefficients are the same when all of the interactions are accounted for explicitly under local equilibrium. This was further demonstrated by comparing a hydrogen-bonding system to one that does not hydrogen bond, which led to insights regarding the use of conventional techniques and the effects caused by solute–solute interactions. These results confirm that time-resolved FTIR-ATR spectroscopy is a powerful tool for accurately measuring diffusion coefficients for both interacting and noninteracting diffusing mixtures in polymers.

Acknowledgment

The authors acknowledge the financial support of the U.S. Army Research Office through Grant DAAD19-00-1-0009 and the Army Research Laboratory Materials Center of Excellence through Grant DAAH04-96-2-0006.

Notation

A_i = integrated absorbance component i in a multicomponent system
$A_{i,\mathrm{eq}}$ = integrated absorbance at equilibrium
A = MEK monomer
AB_n = MEK-BOH complex
B_m = BOH cluster
C_i = concentration of component i in a multicomponent system, mol/cm^3
$C_{i,\mathrm{eq}}$ = concentration at equilibrium, mol/cm^3
d_p = depth of penetration of infrared radiation into the polymer film, cm
D_i = individual diffusion coefficient of component i in a multicomponent system, cm^2/s
$D_{i,\mathrm{eff}}$ = effective diffusion coefficient of component i in a multicomponent system, cm^2/s
k_f = forward rate constant
k_r = reverse rate constant
K = equilibrium constant
L = film thickness, cm
m = size of the BOH cluster (number of BOH monomers)
n = size of MEK-BOH complex (number of BOH monomers per MEK)
t = time, s
z = space, cm

Greek Letters

ϵ^* = effective extinction coefficient for FTIR-ATR spectroscopy, cm^2/mol
θ_i = dimensionless concentration of component i in a multicomponent system
τ = dimensionless time
ζ = dimensionless space

Literature Cited

Aminabhavi, T. M., and R. S. Khinnavar, "Diffusion and Sorption of Organic Liquids Through Polymer Membranes: 10. Polyurethane, Nitrile-Butadiene Rubber and Epichlorohydrin Versus Aliphatic Alcohols (C_1-C_5)," *Polymer*, **34**, 1006 (1993).

Avram, M., and G. D. Mateescu, *Infrared Spectroscopy: Applications in Organic Chemistry*, Wiley, New York (1972).

Balik, C. M., and W. H. Simendinger, "An Attenuated Total Reflectance Cell for Analysis of Small Molecule Diffusion in Polymer Thin Films with Fourier-Transform Infrared Spectroscopy," *Polymer*, **39**, 4723 (1998).

Bellamy, L. J., *The Infra-Red Spectra of Complex Molecules*, Wiley, New York (1958).

Chung, H. S., "The Macedo-Litovitz Hybrid Equation for Liquid Viscosity," *J. Chem. Phys.*, **44**, 1362 (1966).

Cohen, M. H., and D. J. Turnbull, "Molecular Transport in Liquids and Glasses," *J. Chem. Phys.*, **31**, 1164 (1959).

Cussler, E. L., *Multicomponent Diffusion*, Elsevier, Amsterdam (1976).

Danner, R. P., F. Tihminlioglu, R. K. Surana, and J. L. Duda, "Inverse Gas Chromatography Applications in Polymer-Solvent Systems," *Fluid Phase Equil.*, **148**, 171 (1998).

Elabd, Y. A., "Diffusion in Polymers: Penetrant-Polymer and Penetrant-Pentrant Interactions," PhD Thesis, Johns Hopkins Univ., Baltimore, MD (2000).

Elabd, Y. A., and T. A. Barbari, "Separating Solvation from Molecular Diffusion in Polymers," *AIChE J.*, **47**, 1255 (2001).

Grinsted, R. A., and J. L. Koenig, "Study of Multicomponent Diffusion into Polycarbonate Rods Using NMR Imaging," *Macromol.*, **25**, 1229 (1992).

Hong, S. U., T. A. Barbari, and J. M. Sloan, "Diffusion of Methyl Ethyl Ketone in Polyisobutylene: Comparison of Spectroscopic and Gravimetric Techniques," *J. Poly. Sci. Poly. Phys. Ed.*, **35**, 1261 (1997).

Hong, S. U., T. A. Barbari, and J. M. Sloan, "Multicomponent Diffusion of Methyl Ethyl Ketone and Toluene in Polyisobutylene from Vapor Sorption FTIR-ATR Spectroscopy," *J. Poly. Sci. Poly. Phys. Ed.*, **36**, 337 (1998).

Hsu, W. P., R. J. Li, A. S. Myerson, and T. K. Kwei, "Sorption and Diffusion of Water Vapour in Hydrogen-Bonded Polymer Blends," *Polymer*, **34**, 597 (1993).

Kasargod, S. S., and T. A. Barbari, "Permeation Breakthrough Models for Associating and Solvating Penetrants in a Membrane," *Ind. Eng. Chem. Res.*, **36**, 483 (1997).

Lin-Vien, D., N. B. Colthup, W. G. Fateley, and J. G. Grasselli, *The Handbook of Infrared and Raman Characteristic Frequencies of Organic Molecules*, Academic Press, New York (1991).

Macedo, P. B., and T. A. Litovitz, "The Relative Roles of Free Volume and Activation Energy in the Viscosity of Liquids," *J. Chem. Phys.*, **42**, 245 (1965).

Maxwell, J. C., "On the Dynamical Theory of Gases," *Philos. Trans. Roy. Soc.*, **157**, 49 (1867).

Onsager, L., "Reciprocal Relationships in Irreversible Processes," *Phys. Rev.*, **37**, 405 (1931).

Prausnitz, J. M., R. N. Lichtenthaler, and E. G. de Azevedo, *Molecular Thermodynamics of Fluid-Phase Equilibria*, Prentice Hall, Englewood Cliffs, NJ (1986).

Stefan, J., "Über die Dynamische Theorie der Diffusion der Gase," *Wien. Ber.*, **65**, 323 (1872).

Zielinski, J. M., and B. F. Hanley, "Practical Friction-Based Approach to Modeling Multicomponent Diffusion," *AIChE J.*, **45**, 1 (1999).

Manuscript received Aug. 11, 2001, and revision received Jan. 11, 2002.